Article

Influence of Aluminum Laser Ablation on Interfacial Thermal Transfer and Joint Quality of Laser Welded Aluminum–Polyamide Assemblies

Adham Al-Sayyad [1,*] **, Julien Bardon** [2] **, Pierre Hirchenhahn** [3] **, Regis Vaudémont** [2] **, Laurent Houssiau** [3] **and Peter Plapper** [1]

[1] Faculty of Science, Technology and Communication (FSTC), University of Luxembourg, L1359 Luxembourg, Luxembourg; peter.plapper@uni.lu

[2] Materials Research and Technology (MRT), Luxembourg Institute of Science and Technology, L4362 Esch-sur-Alzette, Luxembourg; julien.bardon@list.lu (J.B.); regis.vaudemont@list.lu (R.V.)

[3] Namur Institute of Structured Materials (NISM), LISE laboratory, University of Namur, 5000 Namur, Belgium; pierre.hirchenhahn@unamur.be (P.H.); laurent.houssiau@unamur.be (L.H.)

*   Correspondence: adham.alsayyad@uni.lu; Tel.: +352-466-644-6034

check for updates

Abstract: Laser assisted metal–polymer joining (LAMP) is a novel assembly process for the development of hybrid lightweight products with customized properties. It was already demonstrated that laser ablation of aluminum alloy Al1050 (Al) prior to joining with polyamide 6.6 (PA) has significant influence on the joint quality, manifested in the joint area. However, profound understanding of the factors affecting the joint quality was missing. This work investigates the effects of laser ablation on the surface properties of Al, discusses their corresponding impact on the interfacial thermal transfer between the joining partners, and evaluates their effects on the joint quality. Samples ablated with different parameters, resulting in a range from low- to high-quality joints, were selected, and their surface properties were analyzed by using 2D profilometry, X-ray photoelectron spectroscopy (XPS), scanning electron microscope (SEM), and energy-dispersive X-ray spectroscopy (EDX). In order to analyze the effects of laser ablation parameters on the interfacial thermal transfer between metal and polymer, a model two-layered system was analyzed, using laser flash analysis (LFA), and the thermal contact resistance (TCR) was quantified. Results indicate a strong influence of laser-ablation parameters on the surface structural and morphological properties, influencing the thermal transfer during the laser welding process, thus affecting the joint quality and its resistance to shear load.

1. Introduction

Joining metals to polymers has gained prominent interest among researchers and industries because of its ability to produce lightweight hybrid structures with tailored properties. Conventional metal–polymer joining methods, such as adhesive bonding, mechanical fastening, friction stir welding, and ultrasonic joining, have their drawbacks, as they either require high processing time, involve hazardous chemicals, cause excessive tool wear, involve geometrical constrains, or require the addition of weight to the component. The thermal joining of metals to polymers is challenging because of the significant difference of the thermal properties and melting temperatures of both materials. However, Laser-Assisted Metal–Polymer joining (LAMP) provides the ability to precisely control the energy input into the materials, giving the opportunity to thoroughly melt the polymer at the interface of the joint, while, at the same time, avoiding its degradation. In addition, LAMP has its advantages over

conventional joining methods in being rapid, autogenous, and a non-contact process that offers design flexibility, along with the ability to produce miniaturized joints and minimize overlapping dimensions.

So far, research in LAMP has shown the reliability of the laser welding process in a variety of material combinations [1–4]. Preliminary surface treatments before welding have shown a significant impact on the joint strength and quality. Researchers [3–12] reported the effects of several surface pretreatments on LAMP, including mechanical, chemical, electrochemical, and laser pretreatments for metals, as well as plasma and UV ozone pretreatment for polymers. Similar to adhesive bonding, two main factors were reported in the literature as affecting the LAMP joint properties: mechanical interlocking and physicochemical bonding. However, although LAMP is a thermal joining process, the effect of surface pretreatments on the thermal transfer between the joining partners during the laser welding process, and on the joint quality, has not been investigated.

Increased surface roughness has shown to have a positive effect on enhancing LAMP joint strength by increasing mechanical interlocking effects [9,10,12]. Furthermore, an increased surface roughness might increase the surface wettability of treated metal, which in turns allows a better wetting of the molten polymer during the laser welding process. However, an increase in surface roughness results in an increase in the thermal contact resistance (TCR) across the interface of the two solid materials in contact [13,14]. When two solid surfaces come into contact, the flow of heat across the interface is mainly governed by solid-to-solid conduction at the points of contact, and conduction through the fluid occupying the noncontact area, resulting in restrictions to the heat flow [15]. Yovanovich [16] summarizes forty years of research in the field of thermal contact resistance, and in particular introduces the development of a geometric–mechanical–thermal model called the Cooper–Mikic–Yovanovich (CMY) model to predict the thermal contact resistance of conforming rough surfaces.

Researchers [17–22] developed several theoretical models to calculate thermal contact resistance. Three mechanical models—elastic, plastic, or elastic–plastic deformation of the surface asperities— were considered, assuming that surface asperities follow Gaussian height distributions about a mean plane passing through each surface, and assuming that surface asperities are randomly distributed over the apparent contact area. Yovanovich [23] summarized the TCR model developed by Cooper et al. [20] and proposed compact expression to calculate the TCR between two nominally flat solid surfaces (1 and 2) in contact assuming plastic deformation of asperities as given by Equation (1). Given that σ_1, m_1, k_1 are properties of material 1, and σ_2, m_2, k_2 are properties of material 2, $\sigma = (\sigma_1^2 + \sigma_2^2)^{0.5}$ is the effective root mean square roughness (RMS) so that $\sigma_{1,2} = \sqrt{\frac{1}{L}\int_0^L y^2(x)\mathrm{d}x}$, where L is the profile traced length; $m = (m_1^2 + m_2^2)^{0.5}$ is the effective mean asperity slope, and $m_{1,2} = \frac{1}{L}\int_0^L \left|\frac{\mathrm{d}y(x)}{\mathrm{d}x}\right|\mathrm{d}x$ is the mean absolute asperity slope. H is the microhardness of the softer material, P is the applied pressure, and k_h is the harmonic mean thermal conductivity at the interface where $k_h = 2k_1 k_2/(k_1 + k_2)$. It is clear from Equation (1), which can be utilized in describing the TCR between metal and polymer in their solid state, prior to the laser joining process [24], that TCR has a proportional relation to the ratio of the root mean square roughness σ to the asperities slope, m.

$$TCR = \frac{0.8\sigma}{mk_h}\left(\frac{H}{P}\right)^{0.95} \tag{1}$$

Laser ablation was proven to be an effective and rapid surface pretreatment technique for aluminum (Al 1050) to enhance the bonding strength when welded with polyamide (PA 6.6) [1,5,25]. It was already demonstrated that laser-ablation parameters have a strong impact on the joint quality, demonstrated by the joint area and its resistance to failure, but no effect on the joint strength, i.e., its stress to failure [5]. Results have shown the prominence of cohesive failure mode indicating that interfacial adhesion is not the only factor influencing the joint quality. Preliminary results showed that the joint resistance to failure is influenced by the topography of the ablated aluminum surface, in particular by topography parameters representing the density of peaks on the surface. From the knowledge of TCR models quoted before, it is therefore hypothesized that laser-ablation parameters

affect the thermal transfer between the joining partners, which would reflect on the joint area and quality, impacting its resistance to shear load. This research aims at understanding the effects of surface properties on the interfacial thermal transfer between laser ablated Al 1050 joined to PA 6.6 using laser-beam welding. It correlates the influence of surface topography and the chemistry of aluminum modified layer to the TCR and reports their consecutive effects on the joint quality. To the best of the authors' knowledge, this is the first time that the prominence of the TCR for the welding quality is evidenced in LAMP.

2. Experimental Method

2.1. Materials

In those experiments, 0.5 mm thick EN-AW1050A aluminum (Al) in half-hard state, with geometry of 30 mm × 60 mm, and 4 thick mm polyamide 6.6 (PA) purchased from Dutec (Ahaus, Germany), with the dimensions of 25 mm × 75 mm were used. Prior to the joining process, Al samples were prepared by laser ablation, and PA samples were wiped with ethanol, to remove potential surface contaminants.

2.2. Laser Ablation

Al surfaces were ablated, using a short-pulsed (ns) Nd:YVO4 laser (TruMark 6130 from TRUMPF, Ditzingen, Germany), with a wavelength of 1064 nm and spot size of 45 μm. Al-Sayyad et al. [5] already demonstrated that, from seven different ablation parameters, namely pulse frequency (f_p), beam guidance speed (V), lines, focal position, Al rolling direction, ablation hatching orientation, and laser beam power percentage, only f_p and V had a significant influence on laser welded Al–PA joints' resistance to shear failure. This research focuses on further evaluating the effects of those significant laser-ablation conditions, as shown in Table 1, on Al surface properties, thermal transfer across the joining partners, and corresponding joint quality. Based on previous investigations [5], six ablation conditions (see Table 1) were chosen for this research, as they resulted in a wide range of joint quality. Since ablation was performed with a q-switched laser, increasing pulse frequency results in decreasing the peak pulse power and fluence of the laser beam. However, overlap ratio between consecutive laser pulses (see Figure 1) depends on both pulse frequency and beam guidance speed, as described by Equation (2).

$$O\ (\%) = 100 \times \left(1 - \frac{V\left(\frac{mm}{s}\right)}{f_p\left(\text{Hz}\right) \times O(mm)}\right) \tag{2}$$

Table 1. Laser-ablation parameters and attributes.

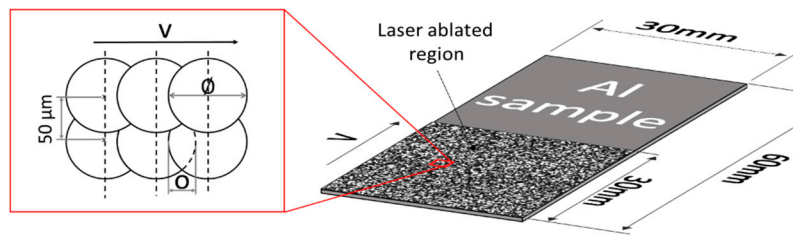| Parameter	Frequency (kHz)	Speed (mm/s)	Peak Pulse Power (kW)	Fluence (J/cm^2)	Overlap Ratio (%)
P1	85	250	11	15.2	93
P2	40	1000	35	28.6	44
P3	70	1000	15	17.9	68
P4	85	1750	11	15.2	54
P5	120	1750	5	9.12	68
P5-95%	Same as Al_5 but with 95% power		4.75	8.66	68

Figure 1. Schematic drawing illustrating six laser pulses irradiating Al surface during laser-ablation process and demonstrating laser pulses overlap ratio (O) between two consecutive pulses.

2.3. Laser-Beam Welding

Laser welding was performed with a fiber laser (TruFiber 400 from TRUMPF), with a wavelength of 1070 nm and a calculated spot size of 58 μm, irradiated on the Al surface after clamping the parts in an overlap configuration, as shown in Figure 2. A peak pulse power of 400 W was modulated with a pulse frequency of 25 kH and pulse duration of 35 μs. The laser beam followed a spiral trajectory, with a feed velocity (v_f) of 88.8 mm/s. Part of the irradiated laser-beam energy gets absorbed, converted to heat energy, conducted through the Al, and transferred to melt PA, thereby joining Al to PA. However, heat transfer across the interface depends on the TCR. Figure 3 shows a simplified illustration of the hypothesized thermal-energy transfer of the irradiated laser beam across the interface in the case of (a) ideal flat surfaces and (b) across rough ablated Al surfaces in contact with smooth PA modeling "real life" conditions. The presence of surface asperities at the interface causes the thermal transfer by conduction to take place mostly at the points of contact [16], thereby increasing TCR and reducing the thermal energy transfer across the interface. Single lap shear tests were performed by using Z010 from Zwick/Roell (Ulm, Germany). Samples were clamped in a vertical alignment, with a jaw-to-jaw distance of 75 mm. The crosshead pulling speed was set at 2.21 mm/min.
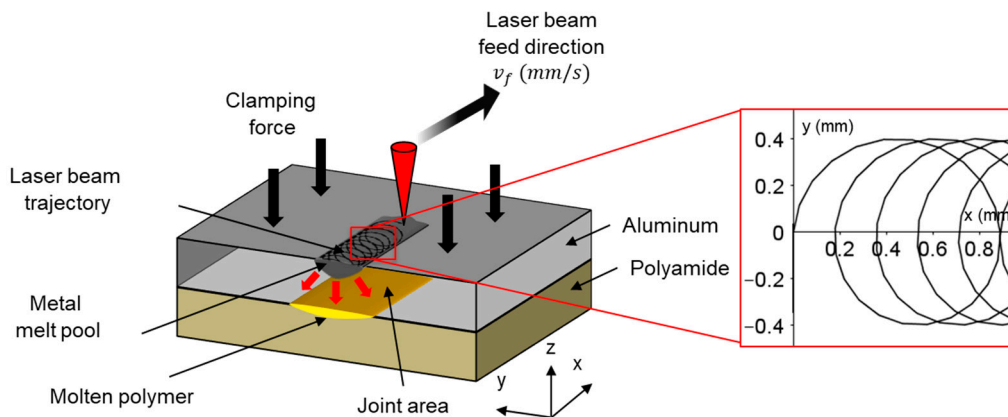

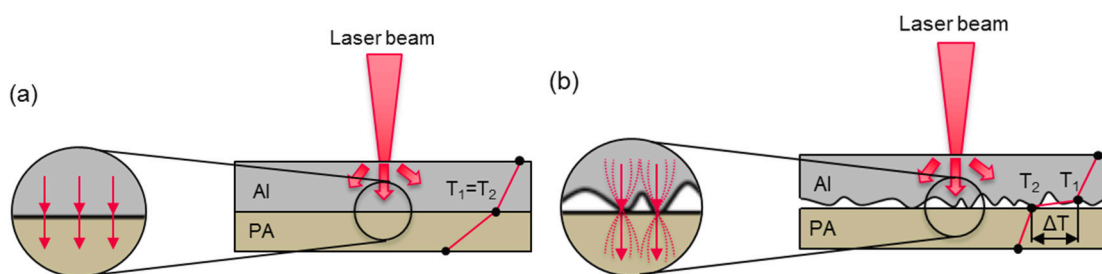**Figure 2.** Schematic drawing of laser-beam-welding setup.

Figure 3. Schematic of hypothesized interfacial thermal-energy transfer during laser-welding process across (**a**) ideally flat conforming surfaces and (**b**) ablated aluminum surfaces in contact with smooth polyamide.

2.4. Joint-Area Assessment

In order to quantify the joint area, a dedicated experimental approach was developed. First, macroscopic images of the joint interface after failure were obtained by using a digital FUJIFILM X-Pro2 camera (Tokyo, Japan). Next, the dimensions of a single pixel were measured, using GIMP software (2.10), by correlating to a predefined scale positioned on the sample close to the weld zone. Then, the coordinates outlining the joint area were allocated, and the joint area was measured by counting the number of pixels and correlating them to the measured pixel dimension. Polarized and stitched microscopic images of the joint area were used to confirm the measurements.

2.5. X-Ray Photoelectron Spectroscopy (XPS)

The atomic composition of treated surfaces and its chemical-bonding states were investigated, using a K-alpha from Thermo Scientific (Waltham, MA, USA). An X-ray beam (Al Kα, 1486.6 eV) with a spot size of 300 μm was used in the analysis. Six regions of 1 cm^2 area were ablated on an Al sample, each region with different ablation condition (see Table 1). Six points per ablated region were investigated by measuring a survey spectrum (3 scans, 200 eV energy pass) and high-resolution spectra for the regions of Al 2*p*, O 1*s*, and C 1*s* (20 scans, 20 eV pass energy) atoms.

2.6. Scanning Electron Microscope (SEM)

A pressure-controlled FEI Quanta FEG 200 scanning electron microscope (SEM) from FEI Company (Hillsboro, OR, USA) was used in secondary electron mode, in order to get information about the samples' morphology. The acceleration voltage was generated at 15 kV. Six regions of 1 cm^2 area were ablated on an Al sample. The sample conductivity was enhanced by depositing a fine layer of conductive lacquer in contact with the untreated aluminum part of the sample. The area that was coated by this lacquer was not observed.

2.7. Energy-Dispersive X-Ray Spectroscopy (EDX)

EDX spectra were obtained in the SEM with an EDAX GENESIS XM 4i energy-dispersive X-ray spectrometer (EDX, Mahwah, NJ, USA). The analytical distance used for X-ray measurement was 10 mm, which corresponded to a take-off angle of 35°. The measurement was performed at a pressure of 3×10^{-4} Pa (water vapor) and an accelerating voltage of 15 kV. A 0.15×0.13 mm^2 area was scanned and an average spectrum was obtained on the whole area. The elemental composition is calculated from this spectrum, assuming the sample is only composed of aluminum, oxygen, and carbon. This assumption is made after observing the whole EDX spectra and identifying the peaks exhibiting a significant height.

2.8. Surface Topography

Surface profile was obtained for the ablated Al by means of a P17 (KLA Tencor, Milpitas, CA, USA) mechanical profilometer equipment with a scanning load of 0.5 mg. Measurements were performed by using acquisition rate of 50 Hz, a scanning speed of 20 μm/s, and a scanning length of 2 mm, resulting in a scanning time of 100 s and 5000 measured points. Six regions of 1 cm^2 area were ablated on an Al sample. Four measurements were performed on each region; two along the axis of applied pulling forces during shear testing, and two perpendicular to it. The roughness profile was calculated with a cut-off length of 0.25 mm. Roughness parameters Rq (average quadratic height or "root-mean-square" roughness) and Rdq (average quadratic slope) were calculated following ISO 4287 [26], and their average value is reported.

Similar measurements performed on PA sample show that its average quadratic height (Rq) is close to 40 nm. Raw or ablated aluminum exhibit Rq values close to 400 nm or in the range of 0.9–6 μm, respectively. It shows that the PA is very smooth compared to ablated aluminum and that the schematic drawing in Figure 3b is a reasonable representation of "real life" conditions.

2.9. Laser Flash Analysis (LFA)

In order to prepare ablated samples for LFA, they were cut to 1 cm^2 squared geometry, using an Accutom 50 dicing tool from Struers (Ballerup, Denmark). Then, ablated samples were arranged in layered configuration, together with a 1 mm thick polished aluminum sample with the same dimensions as the ablated ones, as shown in Figure 4. Samples were coated on both external faces using Graphit 33 spray from Kontakt Chemie (Iffezheim, Germany) containing 1–5 *w/w* % of graphite powder in order to have a consistent absorbance to the laser beam and consistent emissivity to the IR detector.

Laser flash analysis (LFA) test was performed by a Netzsch LFA 457 Microflash machine (Selb, Germany) at room temperature. A single flash (0.5 ms) from Nd-Yag laser was irradiated on the untreated surface of the ablated aluminum sample, as illustrated in Figure 4. The LFA chamber was filled with dry argon gas during the experimentation in order to reduce the influence of moisture on the measurement of the thermal properties. An infrared detector (InSb photodiode) was used to monitor the temperature transient at the back face. The output voltage of the laser was fixed at 1922 V for all experiments. A duration of 60 ms was used for the acquisition time of the IR detector.

Layered configuration (see Figure 4) was used in order to calculate the TCR generated by the particular geometry of the rough ablated surface in contact with a flat surface [27]. It is difficult to calculate the exact TCR between PA and Al by using LFA with such layered configuration, due to experimental challenges resulting from the low thermal conductance of PA. Therefore, the rough ablated aluminum is brought into contact with another flat aluminum sample. Thermal diffusivity of the layered system is evaluated from the measurement of temperature increase as a function of time at the back face of the polished aluminum, i.e., the side facing the IR sensor. Then, the density, thickness, thermal diffusivity, and specific heat of both materials were predefined to that of pure aluminum, kept constant for all tested samples, and used to calculate the TCR based on the algorithm developed by Hartmann et al. [28].
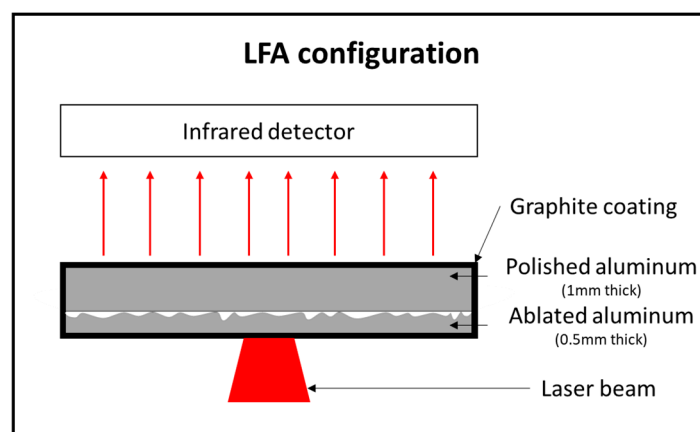

Figure 4. Schematic drawing of laser flash analysis layered configuration.

3. Results

3.1. Joint Strength

The joint area was identified at the joint interface after failure as the area of residues/damages on both materials. The joint area measured in the case of ethanol-wiped aluminum (Al ref) showed 58% of the joint area measured on the corresponding PA indicating a mixture between adhesive and cohesive failure modes. Figure 5 plots the joint area versus shear load at failure for samples that had their aluminum ablated prior to the joining process with the six parameters discussed in this article. Although shear load at failure of the tested samples varies from 524 to 1632 N, linear relation between joint area and shear load indicates constant strength across all samples. A descriptive model

was generated to describe the relation between all data points. High coefficient of determination (R^2) of 0.98 illustrates very low variability in the calculated strength, as indicated by a slope of 34.69 MPa. In addition, results show equal and matching joint area on corresponding Al and PA samples, demonstrating prominence of cohesive failure mode for the ablated aluminum and indicating that the reported variation in joint quality is less likely to be a result of variations in interfacial chemical-bonding behavior. Results confirm that laser-ablation parameters have a significant influence on the joint quality, manifested in the joint area as shown in Figure 6, but no influence on the joint strength. Table 2 shows the effect of laser-ablation parameters on joint resistance to shear load.
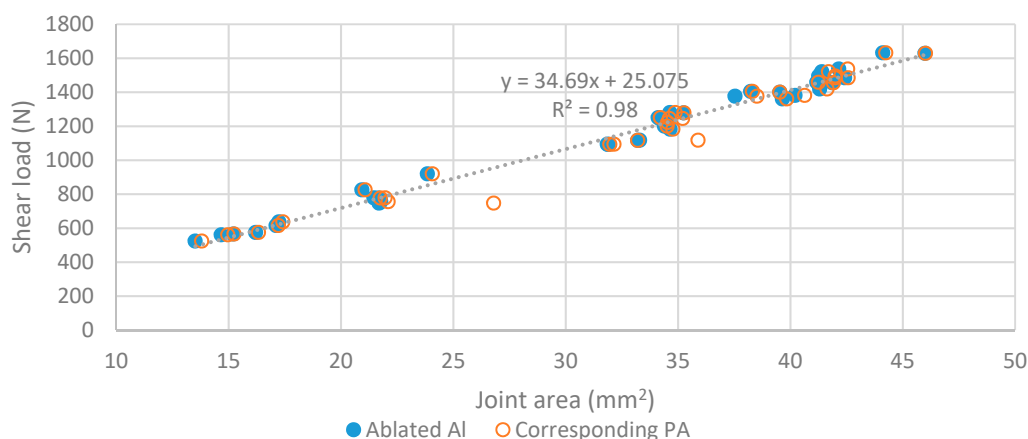
Figure 5. Evolution of joint area, along with increasing joint's resistance to failure.

Figure 6. Stitched microscopic images of PA joint area after failure (dark areas), illustrating effect of laser-ablation parameters on joint quality.

Table 2. Effect of laser-ablation parameters on joint resistance to failure.

Ablation Parameters	P1	P2	P3	P4	P5	P5-95%
Average shear load (N)	580 ± 41	800 ± 65	1222 ± 143	1341 ± 172	1415 ± 113	1465 ± 65

3.2. X-Ray Photoelectron Spectroscopy (XPS)

As far as the general composition of the treated aluminum surfaces (see Figure 7) is concerned, it is first observed that laser ablation removes a large part of the adsorbed carbon on the surface, as well as other impurities, resulting in a "cleaning" effect. Concerning the sample which had its surface wiped only with ethanol (Al ref), a high carbon content is visible (29.5 at.%) and a relatively low oxygen concentration (41.1 at.%). After laser pretreatment, a significant decrease in the carbon content on the surface could be noticed, along with an increase in oxygen content. It corresponds to the effects which are generally expected for laser ablation of aluminum: the high energy density of the laser beam has two possible effects, either acting separately or in combination. First, laser ablation certainly causes the

removal of surface contaminants, thereby lowering the "masking" effect of the aluminum surface by the contamination top layer. Second, it might contribute to the regeneration of a thicker oxide layer on the Al surface due to high surface temperature during the ablation process. While a minor nitrogen content of 0.7, 0.7, and 0.5 at.% was detected on P1, P2, and P3, samples ablated with parameters P4, P5, and P5-95% illustrated the presence of only aluminum, oxygen, and carbon elements.

Surface chemistry of the different laser-ablated samples do not significantly differ in aluminum, oxygen, and carbon composition. Since no metallic aluminum at 72.7 eV can be found in the high-resolution Al 2*p* spectra of the ablated samples, Strohmeier's method [29] cannot be used to estimate the oxide thickness. The oxide of the reference samples thickness has been estimated at 5.5 nm by using this method. This implies that the oxide layer is much thicker than the depth limit probed in XPS, which is evaluated in its wide range at 20 nm [30]. The details of the high-resolution spectra of the different elements (C 1*s*, O 1*s*, and Al 2*p*) were very similar across the ablated surfaces, meaning that the surface chemistry is almost identical regardless of the laser-ablation parameters and the resulted joint's strength.
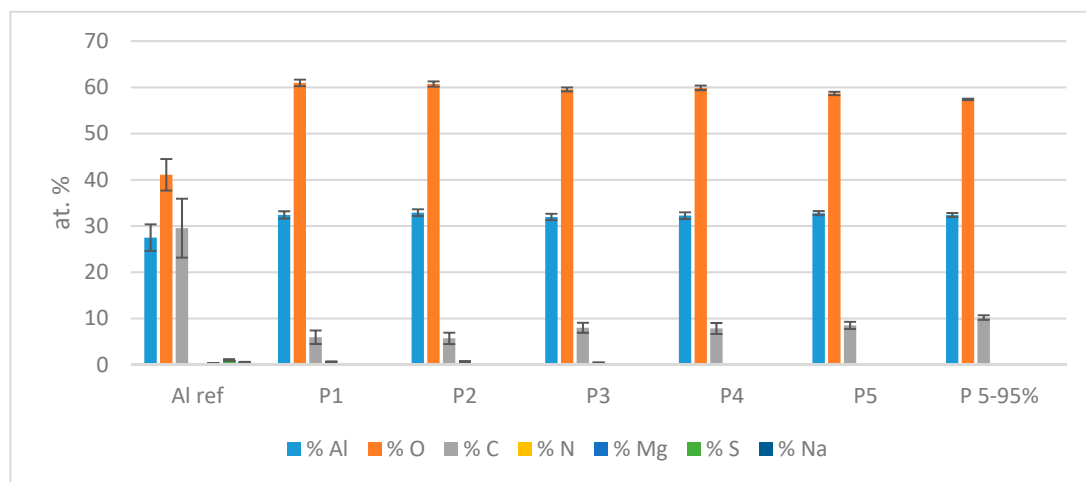

Figure 7. XPS elemental composition of aluminum surfaces.

3.3. Scanning Electron Microscope (SEM)

SEM results shown in Figure 8 illustrates the morphology of the aluminum oxide resulted from the laser-ablation process. The red square shown in 1000× magnification illustrates the area where EDX analysis was performed. Samples ablated with parameter P1, which demonstrated the lowest joint quality, shows relatively high peaks and deep valleys with relatively coarse structures. However, as the joint quality increases, ablated aluminum surfaces are shown to exhibit a smoother surface with finer peak structures, as can be clearly seen on sample P5-95, which resulted in the highest average resistance to failure. Since the failure occurs close to the Al–PA interface (typically 10–15 μm in depth in the PA), the influence of mechanical interlocking cannot be excluded a priori. However, it would be expected that a rougher surface is responsible for a greater mechanical interlocking, thereby reinforcing the joint. The opposite effect is observed here, i.e., the samples exhibiting higher roughness show lower joint quality. It is therefore assumed that mechanical interlocking does not govern the difference of joint resistance to failure.
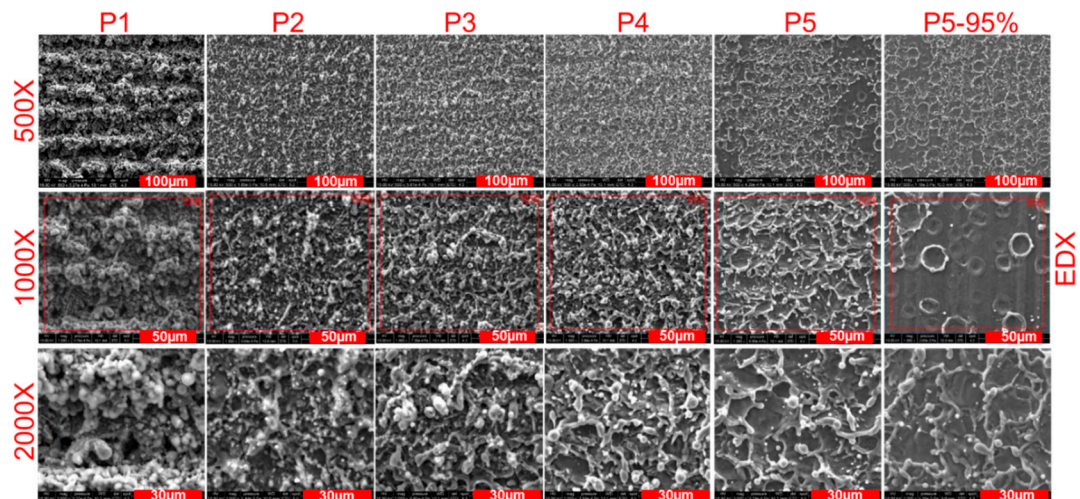
Figure 8. SEM images of ablated surfaces.

3.4. Energy-Dispersive X-Ray Spectroscopy (EDX)

EDX results shown in Figure 9 illustrate atomic percentage of oxygen, carbon, and aluminum. While XPS analyzes a depth which is smaller than 20 nm [30], EDX depth of analysis with the current EDX parameters in use and in case of aluminum oxide would yield a depth close to 2 μm. The carbon element cannot be correctly quantified by the EDX technique and will not be considered in this study.
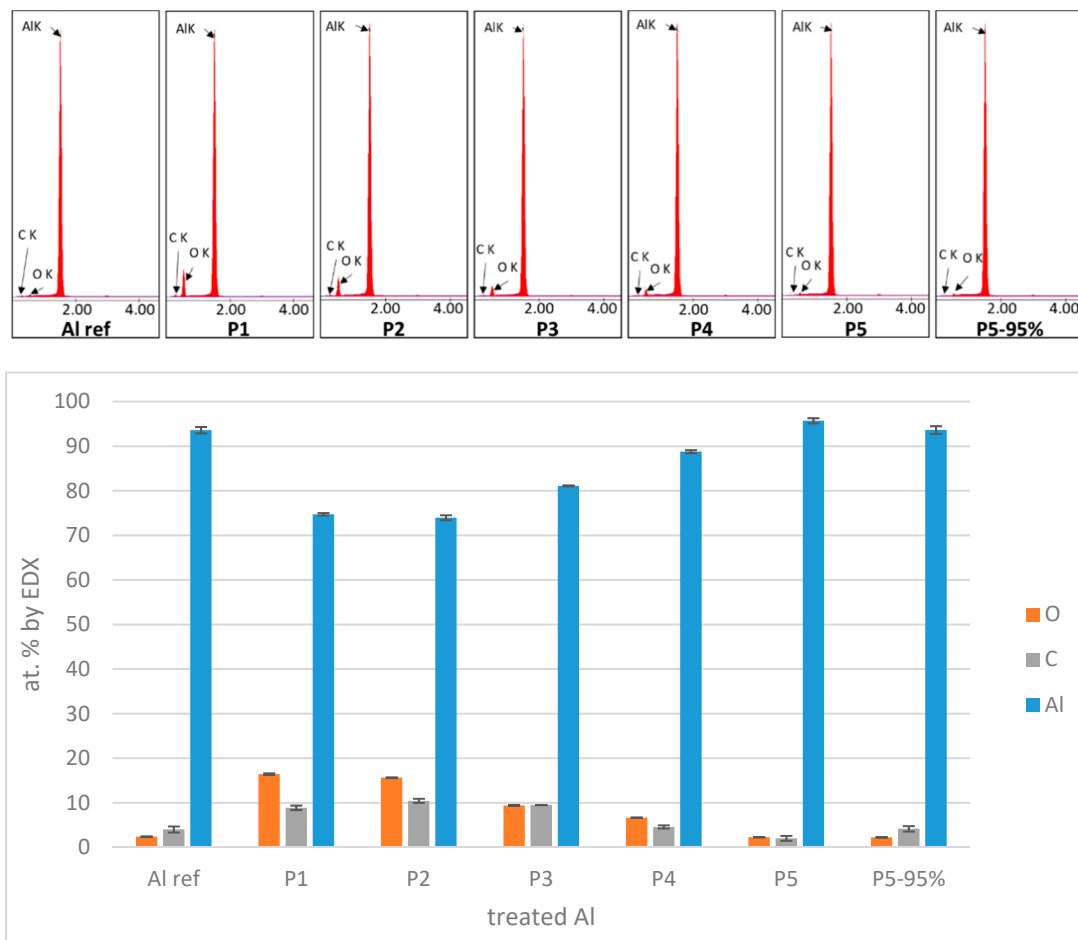

Figure 9. EDX elemental composition of aluminum surfaces.

Interestingly, oxygen concentration detected by EDX increases for the ablation condition. More precisely, this increase is very significant for ablation conditions P1 and P2 (16.4% and 15.6%, respectively), and it is significant to a lesser extent for P3 and P4 (9.4% and 6.7%, respectively), compared to untreated aluminum (2.4%). This leads to the assumption that oxidation of aluminum occurs for ablation conditions P1 to P4 and is particularly large for conditions P1 and P2. This is consistent with XPS results that lead to the conclusion that oxidation occurs at a larger depth than 20 nm for conditions P1 to P4.

A decline in the oxygen peak intensity along the ablated samples from P1 to P5 suggests a decline in aluminum oxide and/or hydroxide layer thickness along the ablation conditions (P1 to P5). EDX is not conclusive for conditions P5 and P5-95%, probably because it is not precise enough at these low concentrations of oxygen (close to 2.4%).

3.5. Surface Topography

The reference aluminum (cleaned with ethanol) exhibited relatively low surface roughness ($Rq = 0.43 \pm 0.26$ µm). Regarding the laser-ablated Al, several topography parameters' values were investigated for correlations with the achieved joint quality. However, no strong correlation was found between Rdq, Rq, and the joint's resistance to failure indicated by the Pearson correlation coefficients of -0.77 and -0.83, respectively. Figure 10 shows the relation between roughness profile parameters ratio Rq/Rdq involved in the TCR model (Equation (1)) with the corresponding joint's resistance to failure, where σ reflects Rq (µm) and m reflects Rdq measured on ablated aluminum surfaces. The correlation between ratio Rq/Rdq and joint's resistance indicated by the Pearson correlation coefficient is -0.93.
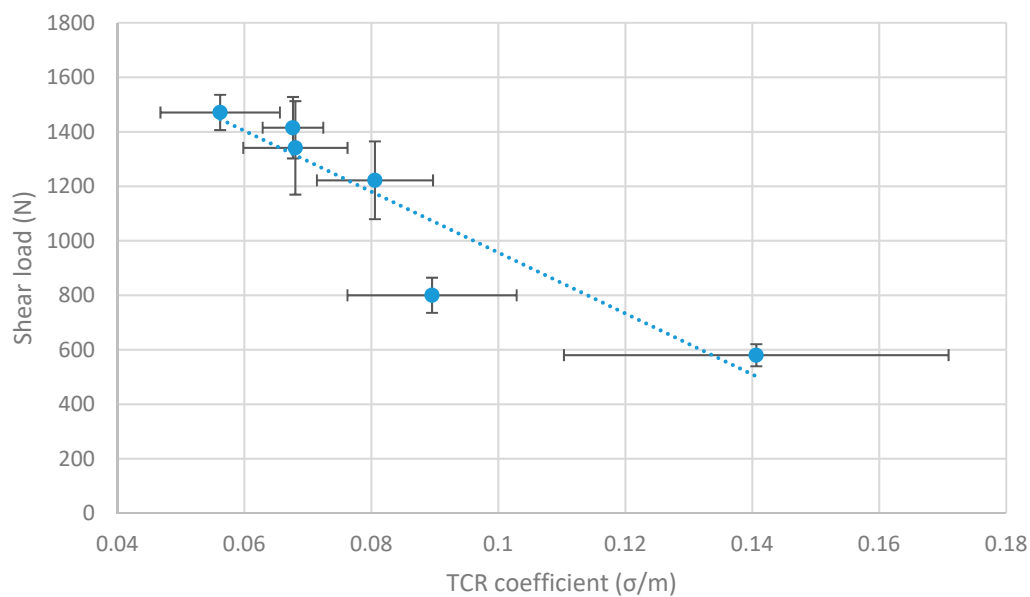

Figure 10. Relation between surface topography and joint's resistance to failure.

3.6. Laser Flash Analysis

In order to fully understand the combined effects of laser-ablation parameters on the thermal transfer through a rough Al surface, LFA layered tests were conducted. Results in Figure 11 show that a decreased TCR across the interface of the layered setup correlates significantly with an increase in the joint's resistance to failure, with a Pearson correlation coefficient of $r = -0.94$. Results confirm that the improvement in joint quality, which is manifested by enhanced joint area and increased resistance to failure, is very likely to be a result of reduced TCR across the interface of the joining partners during the welding process.
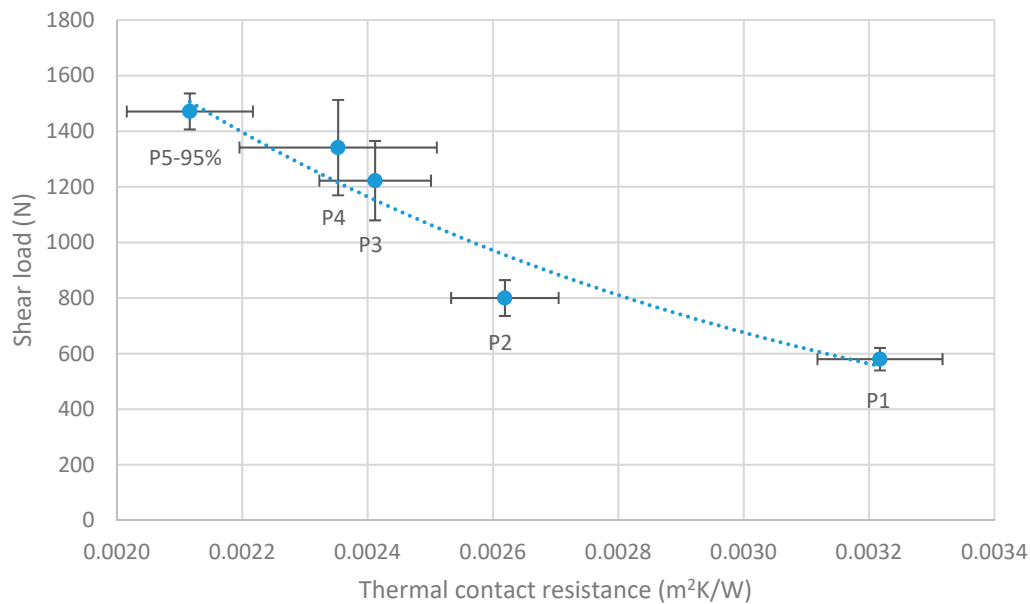
Figure 11. Relation between thermal contact resistance and joint's resistance to failure.

4. Discussion

The lower mechanical resistance of the joint for untreated (reference, only ethanol cleaning) aluminum compared to laser-ablated samples is easily linked to the different surface chemistry. More precisely, laser ablation is responsible to a lower level of carbon contamination and the formation of a relatively thick oxide layer on aluminum. This certainly creates a strong interaction with molten PA during welding, resulting in cohesive failure mode. This is not the case for reference aluminum, which is responsible for the observation of areas of adhesive failure at the interface, thereby reducing the joint resistance.

The difference in joint resistance between laser-ablation conditions clearly comes from a difference in joint area, as stated in 3.1. However, this difference in joint area is difficult to explain. When surface chemistry (as evaluated by XPS) is considered, the only correlation that can be observed is a slight increase of carbon content and a slight decrease of oxygen content from P1 to P5-95, i.e., when shear load increases. An increase in carbon content at the aluminum surface is expected to weaken the interactions at the interface between aluminum and PA and makes the joint weaker. This is contradictory to what is actually observed, in particular if it is also mentioned that failure for ablated samples occurs in PA (cohesive failure), i.e., adhesion at the interface is certainly not responsible for the failure of the assembly.

Interestingly, two good correlations between ablated aluminum properties and shear load are observed. The first one is the decrease of the oxygen concentration, as evaluated by EDX, when shear load increases, and the second is the decrease of Rq/Rdq ratio when shear load increases.

The inverse correlation (Pearson coefficient $r = -0.98$) between EDX oxygen concentration and shear load could probably be explained by a different thermal behavior of the aluminum sample as a function of its content of oxide or hydroxide relatively to metal aluminum. For instance, if it is hypothesized that aluminum oxide is more stable than hydroxide and that it is formed as a layer close to the surface of aluminum, then the aluminum sample can be considered as a two-layer system: metal aluminum in the bulk and aluminum oxide layer at the surface. Since the thermal diffusivity of aluminum oxide (12 mm^2/s) is lower than pure aluminum (94 mm^2/s) at 300 K [31], this means that a thicker aluminum oxide layer would act as a larger thermal insulator for the transmission of heat to PA during welding. Thus, an increase in oxygen concentration would result in a decrease in volume of molten polymer during welding, leading to a smaller joint area and a decline in the joint's resistance to failure.

Otherwise, the inverse correlation between the *Rq/Rdq* ratio and shear load (Pearson's correlation $r = -0.93$) has to be interpreted in the light of Equation (1), which links the thermal contact resistance and the σ/m ratio as a surface topography characteristic. In terms of phenomena, it means that, when thermal conduction across a "rough interface" (see Figure 3b) is governed by the area of microcontacts, the thermal contact resistance (TCR) increases as the area of microcontacts decreases. A lower value of *Rq/Rdq* ratio leads to a lower value of TCR, meaning that a greater heat flow is conducted across the interface. This leads to the melting of a greater volume of PA during welding, which results in a larger joint and a larger shear load. Furthermore, the fact that TCR evaluated by LFA experiments following Hartmann's method is also well correlated to shear load makes these arguments stronger.

Both phenomena (thermal insulation by aluminum oxide and change of TCR by means of different topography) convincingly explain the increase in shear load from P1 to P5-95. Nevertheless, the authors are currently not able to quantify which phenomenon has the larger effect on this increase, or if one of the two phenomena shall be neglected. Further investigations shall be necessary to answer this question.

Moreover, the correlation between topography and shear load explains why, a posteriori, no correlation was found between the *Ra* topography value (which is strongly correlated to *Rq* value) and shear load in our former article [5]. In such a case, the critical characteristic of the surface topography is its morphology of peaks, evaluated by *Rq/Rdq* ratio, and not its amplitude, which is evaluated by *Ra* or *Rq*.

5. Conclusions

The link between the aluminum surface characteristics after laser ablation and the shear resistance of dissimilar joints formed by laser welding of ablated aluminum with polyamide was investigated. It is observed that shear load at failure of the joint depends on the joint area demonstrating constant joint strength regardless of the ablation parameters. Good correlations between surface characteristics and shear load lead us to make two possible assumptions for explaining the reduction in joint area.

First, it is observed that laser ablation leads to a significant increase of oxygen content in the first micrometers (in depth) of aluminum surface. This might be responsible for a reduction of thermal conduction in the oxygen-rich volume (formation of aluminum oxide/hydroxide), which in turn reduces the quantity of heat transmitted to melt PA during welding.

Second, it is observed that the different topography characteristics obtained after laser ablation of aluminum exhibit different morphology of peaks, which might in turn influence the thermal contact resistance (TCR) between the rough aluminum and the flat PA during welding.

Experimental evaluation of TCR by LFA confirms that thermal-transfer phenomena are probably responsible of changes in shear-load resistance.

This article shed light on the prominence of interfacial thermal-transfer phenomena in the quality of joints obtained by laser welding of a rough ablated aluminum with a polymer.

References

1. Lamberti, C.; Solchenbach, T.; Plapper, P.; Possart, W. Laser assisted joining of hybrid polyamide-aluminum structures. *Phys. Procedia* **2014**, *56*, 845–853. [CrossRef]

2. Katayama, S.; Kawahito, Y. Laser direct joining of metal and plastic. *Scr. Mater.* **2008**, *59*, 1247–1250. [CrossRef]

3. Wahba, M.; Kawahito, Y.; Katayama, S. Laser direct joining of AZ91D thixomolded Mg alloy and amorphous polyethylene terephthalate. *J. Mater. Process. Technol.* **2011**, *211*, 1166–1174. [CrossRef]

4. Arai, S.; Kawahito, Y.; Katayama, S. Effect of surface modification on laser direct joining of cyclic olefin polymer and stainless steel. *Mater. Des.* **2014**, *59*, 448–453. [CrossRef]

5. Al-Sayyad, A.; Bardon, J.; Hirchenhahn, P.; Santos, K.; Houssiau, L.; Plapper, P. Aluminum pretreatment by a laser ablation process: Influence of processing parameters on the joint strength of laser welded aluminum—Polyamide assemblies. *Procedia CIRP* **2018**, *74*, 495–499. [CrossRef]

6. Bergmann, J.P.; Stambke, M. Potential of laser-manufactured polymer-metal hybrid joints. *Phys. Procedia* **2012**, *39*, 84–91. [CrossRef]

7. Zhang, Z.; Shan, J.G.; Tan, X.H.; Zhang, J. Effect of anodizing pretreatment on laser joining CFRP to aluminum alloy A6061. *Int. J. Adhes. Adhes.* **2016**, *70*, 142–151. [CrossRef]

8. Klotzbach, A.; Langer, M.; Pautzsch, R.; Standfuß, J.; Beyer, E. Thermal direct joining of metal to fiber reinforced thermoplastic components. *J. Laser Appl.* **2017**, *29*, 022421. [CrossRef]

9. Amend, P.; Pfindel, S.; Schmidt, M. Thermal joining of thermoplastic metal hybrids by means of mono- and polychromatic radiation. *Phys. Procedia* **2013**, *41*, 98–105. [CrossRef]

10. Holtkamp, J.; Roesner, A.; Gillner, A. Advances in hybrid laser joining. *Int. J. Adv. Manuf. Technol.* **2010**, *47*, 923–930. [CrossRef]

11. Georgiev, G.L.; Baird, R.J.; McCullen, E.F.; Newaz, G.; Auner, G.; Patwa, R.; Herfurth, H. Chemical bond formation during laser bonding of Teflon® FEP and titanium. *Appl. Surf. Sci.* **2009**, *255*, 7078–7083. [CrossRef]

12. Roesner, A.; Scheik, S.; Olowinsky, A.; Gillner, A.; Reisgen, U.; Schleser, M. Laser assisted joining of plastic metal hybrids. *Phys. Procedia* **2011**, *12*, 373–380. [CrossRef]

13. Cui, T.; Li, Q.; Xuan, Y. Characterization and application of engineered regular rough surfaces in thermal contact resistance. *Appl. Therm. Eng.* **2014**, *71*, 400–409. [CrossRef]

14. Zhang, P.; Cui, T.; Li, Q. Effect of surface roughness on thermal contact resistance of aluminium alloy. *Appl. Therm. Eng.* **2017**, *121*, 992–998. [CrossRef]

15. Prasher, R. Thermal interface materials: Historical perspective, status, and future directions. *Proc. IEEE* **2006**, *94*, 1571–1586. [CrossRef]

16. Yovanovich, M.M. Four decades of research on thermal contact, gap, and joint resistance in microelectronics. *IEEE Trans. Compon. Packag. Technol.* **2005**, *28*, 182–206. [CrossRef]

17. Greenwood, J.A.; Williamson, J.B.P. Contact of nominally flat surfaces. *Proc. R. Soc. London Ser. A Math. Phys. Sci.* **1966**, *295*, 300–319. [CrossRef]

18. Greenwood, J.A. The area of contact between rough surfaces and flats. *J. Lubr. Technol.* **1967**, *89*, 81–87. [CrossRef]

19. Greenwood, J.A.; Tripp, J.H. The contact of two nominally flat rough surfaces. *Proc. Inst. Mech. Eng.* **1970**, *185*, 625–633. [CrossRef]

20. Cooper, M.G.; Mikic, B.B.; Yovanovich, M.M. Thermal contact conductance. *Int. J. Heat Mass Transf.* **1969**, *12*, 279–300. [CrossRef]

21. Mikić, B.B. Thermal contact conductance; theoretical considerations. *Int. J. Heat Mass Transf.* **1974**, *17*, 205–214. [CrossRef]

22. Sayles, R.S.; Thomas, T.R. Thermal conductance of a rough elastic contact. *Appl. Energy* **1976**, *2*, 249–267. [CrossRef]

23. Yovanovich, M.M.; Marotta, E.E. Thermal spreading and contact resistances. In *Heat Transfer Handbook*; Bejan, A., Kraus, A.D., Eds.; Wiley: Hoboken, NJ, USA, 2003; pp. 261–395.

24. Bahrami, M.; Yovanovich, M.M.; Marotta, E.E. Thermal joint resistance of polymer-metal rough interfaces. *J. Electron. Packag.* **2006**, *128*, 23. [CrossRef]

25. Al-Sayyad, A.; Bardon, J.; Hirchenhahn, P.; Mertz, G.; Haouari, C.; Houssiau, L.; Plapper, P. Influence of laser ablation and plasma surface treatment on the joint strength of laser welded aluminum-polyamide assemblies. In Proceedings of the JNPLI 2017, Strasbourg, France, 13–14 September 2017.

26. *ISO 4287–Geometrical Product Specifications (GPS)—Surface Texture: Profile Method—Terms, Definitions and Surface Texture Parameters*; International Organization for Standardization: Geneva, Switzerland, 1997.

27. Corbin, S.F.; Turriff, D.M. Thermal diffusivity by the laser flash technique. *Charact. Mater.* **2002**. [CrossRef]

28. Hartmann, J.; Nilsson, O.; Fricke, J. Thermal diffusivity measurements on two-layered and three-layered systems with the laser-flash method. *High Temp. Press.* **1993**, *25*, 403.

29. Strohmeier, B.R. An ESCA method for determining the oxide thickness on aluminum alloys. *Surf. Interface Anal.* **1990**, *15*, 51–56. [CrossRef]

30. Ratner, B.D.; Castner, D.G. Electron spectroscopy for chemical analysis. In *Surface Analysis—The Principal Techniques*; John Wiley & Sons, Ltd.: Chichester, UK, 2009; pp. 47–112.

31. King, J.A. *Materials Handbook for Hybrid Microelectronics*; Artech House: Boston, MA, USA, 1988.